

1 **A topside equatorial ionospheric density and**
2 **composition climatology during and after extreme**
3 **solar minimum**

J. H. Klenzing,¹ F. Simões,¹ S. Ivanov,² R. A. Heelis,³ D. Bilitza,^{4,5} R. F.

Pfaff,¹ and D. E. Rowland¹

J. H. Klenzing, Space Weather Lab / Code 674, Goddard Space Flight Center, Greenbelt,
Maryland, USA (jeffrey.klenzing@nasa.gov)

¹Space Weather Lab / Code 674,
Goddard Space Flight Center, Greenbelt,
Maryland, USA

²Department of Physics, Georgia Institute
of Technology, Atlanta, Georgia, USA

³Center for Space Sciences, University of
Texas at Dallas, Richardson, Texas, USA

⁴Heliophysics Laboratory / Code 672,
Goddard Space Flight Center, Greenbelt,
Maryland, USA

⁵Department of Physics, George Mason
University, Fairfax, Virginia, USA

4 **Abstract.** During the recent solar minimum, solar activity reached the
5 lowest levels observed during the space age. This extremely low solar activ-
6 ity has accompanied a number of unexpected observations in the Earth's iono-
7 sphere and thermosphere when compared to previous solar minima. Among
8 these are the fact that the ionosphere is significantly contracted beyond ex-
9 pectations based on empirical models. Climatological altitude profiles of ion
10 density and composition measurements near the magnetic dip equator are
11 constructed from the C/NOFS satellite to characterize the shape of the top-
12 side ionosphere during the recent solar minimum and into the new solar cy-
13 cle. The variation of the profiles with respect to local time, season, and so-
14 lar activity are compared to the IRI-2007 model. Building on initial results
15 reported by *Heelis et al.* [2009], here we describe the extent of the contracted
16 ionosphere, which is found to persist throughout 2009. The shape of the iono-
17 sphere during 2010 is found to be consistent with observations from previ-
18 ous solar minima.

1. Introduction

19 The solar minimum between cycles 23 and 24 has been an unusual period of solar activ-
20 ity. The minimum was expected to occur in 2006, but instead solar activity continually
21 decreased throughout 2007 and 2008 [*Russell et al.*, 2010]. Traditional proxies for solar ac-
22 tivity such F10.7 (the flux of solar radiation at 10.7 cm wavelength) have “bottomed out,”
23 while actual measurements of the EUV flux have continued to decrease [*Araujo-Pradere*
24 *et al.*, 2011; *Chen et al.*, 2011]. Some long-term climate modelers have even speculated
25 that the deepest part of this minimum could be used to better understand the Maunder
26 minimum [*Schrijver et al.*, 2011].

27 A number of surprising observations in the ionosphere and thermosphere has accom-
28 panied this period of extremely low solar activity. The thermospheric density was found
29 to reach record lows based on the analysis of the orbital decay of numerous satellites
30 [*Emmert et al.*, 2010] and by *in situ* measurement of the neutral scale-height [*Haaser et*
31 *al.*, 2010]. *Solomon et al.* [2011] showed that this reduction in thermospheric density was
32 largely due to low solar activity and that other secular variations (such as geomagnetic
33 activity) were small in comparison.

34 *Heelis et al.* [2009] showed that the ionosphere was contracted as well, with the transition
35 height between H⁺ and O⁺ being significantly lower than predicted by the IRI model.
36 Additionally, the topside nighttime ion temperatures have been found to be relatively
37 cold compared to IRI at an altitude of 400 km, as low as 600 K [*Coley et al.*, 2010]. The
38 average ion drift in the topside ionosphere has been found to be significantly different
39 from previous observations, including other solar minima. The $\mathbf{E} \times \mathbf{B}$ drift climatology

40 observed by the C/NOFS satellite was found to differ from the Fejer-Scherliess model
41 [*e.g.*, *Scherliess and Fejer*, 1999], including downward afternoon drifts in some regions as
42 well as a weak to non-existent pre-reversal enhancement [*Pfaff et al.*, 2010].

43 The behavior of the topside ionosphere during solar minimum has been well-documented
44 through *in situ* measurements [*Greenspan et al.*, 1994; *West et al.*, 1997], topside sounders
45 [*Benson and Bilitza*, 2009], and ground-based radar [*Hysell et al.*, 2009]. However, because
46 solar activity is lower during the cycle 23/24 minimum than during the last few solar
47 cycles, current empirical models must extrapolate based on previous observations. Long-
48 term monitoring of ionospheric density by the CHAMP and GRACE satellites reveal that
49 the IRI-2007 model overestimates the expected density leading up to and including the
50 recent solar minimum [*Lühr and Xiong*, 2010].

51 In this study, the ion density and composition data from the C/NOFS satellite are used
52 to construct climatological maps of density and composition as a function of altitude and
53 local time near the magnetic dip equator. The maps are divided into season and solar
54 activity in order to understand the shape of the topside ionosphere during this extreme
55 solar minimum, as well as its evolution on the journey back to solar maximum. These
56 climatology maps are compared to the results from the IRI-2007 model. The highly
57 contracted ionosphere is found to persist throughout 2009, well into the new solar cycle.

2. Measurements and Models

58 The Communication/Navigation Outage Forecast System (C/NOFS) satellite is part of
59 a space weather mission led by the US Air Force Research Laboratory to locate, under-
60 stand, and predict equatorial ionospheric scintillation [*de La Beaujardière et al.*, 2004].
61 The C/NOFS satellite was launched in April 2008 into a 13° inclination orbit with perigee

62 near 400 km and apogee near 860 km. This elliptical orbit allows for a sampling of ion
63 density over multiple scale heights of the topside ionosphere. The C/NOFS perigee pre-
64 cesses through all solar local times roughly once every 65 days. C/NOFS is equipped with
65 multiple instrument suites designed to study the ion and neutral populations and their
66 effect on the propagation of communication signals.

67 This study will focus on the total ion density (electron density for a quasi-neutral
68 plasma) and the H^+ and O^+ components. The total density and composition are obtained
69 from a Retarding Potential Analyzer (RPA), part of the Coupled Ion-Neutral Dynamics
70 Investigation (CINDI) suite of instruments on board C/NOFS. The well-established RPA
71 technique consists of using a series of biased grids to select certain energies of ions to
72 measure as a current [*Heelis and Hanson, 1998*]. By sweeping over a range of voltages,
73 the relative contribution of each ion species (along with ion drift velocity and temperature)
74 can be calculated.

75 The International Reference Ionosphere (IRI) is considered the international standard
76 model for calculating empirically-derived ionospheric parameters based on both ground-
77 based and satellite measurements [*Bilitza and Reinisch, 2008*]. IRI was founded as a joint
78 project between the Committee on Space Research (COSPAR) and by the International
79 Union of Radio Science (URSI). An empirical model was chosen for comparison to the
80 C/NOFS observations in order to better illustrate the differences between the topside
81 density variations when compared to previous solar minima. The IRI model can generate
82 estimated values of density and ion composition for a given input of solar activity, which
83 is described by the geophysical indices Rz (based on the sunspot number) and IG (based
84 on the ionospheric response) [*Bilitza, 2000*].

85 The international sunspot number (Rz, also referred to as Ri after the main observation
86 platform moved from Zürich to Brussels in 1980) is a weighted average of the number of
87 sunspots observed on the surface of the sun [Clette *et al.*, 2007]. The weighting is designed
88 to account for the differences between individual sunspots and clusters of sunspots. The
89 IG index was developed by Liu *et al.* [1983] to provide an estimate of the peak F2-region
90 density based on the International Radio Consultative Committee (CCIR) maps of the
91 ionosphere. To do this, the index uses a weighted average of ionosonde measurements
92 around the world similar to the method introduced by Minnis and Bazzard [1960]. This
93 index is scaled to produce a “global effective sunspot number.” However, since this cal-
94 culation is based on the actual measurements of the ionosphere, it does not have a lower
95 limit (unlike Rz, which by definition cannot be less than zero). During the prolonged solar
96 minimum between cycles 23 and 24, IG is often negative. The IG index is provided by
97 the UK World Data Center and is available in either monthly averages (IG) or 12-month
98 averages (IG₁₂).

99 The NeQuick topside model is used to generate expected values of ion density and
100 composition every five seconds along the orbit track of C/NOFS for every orbit through
101 the end of 2010. The NeQuick model was chosen due to its excellent performance when
102 compared to topside sounder measurements from the Alouette and ISIS missions relative
103 to the other topside options included in IRI [Bilitza *et al.*, 2006; Bilitza, 2009]. For this
104 study, the 12-month running averages of Rz (referred to as Rz₁₂) and IG (IG₁₂) are used.
105 Only dates with the definitive values of Rz₁₂ and IG₁₂ (through January 2011 at the time
106 of this writing) were used.

107 To illustrate the prolonged nature of the recent solar minimum, these activity proxies
108 are compared for the last three solar cycles in Figure 1. Panel (a) shows the values of
109 F10.7A (the 81-day average of F10.7) for 36 months around the minima between cycles
110 20 and 21 (1975, plotted in blue), cycles 21 and 22 (1986, plotted in green), cycles 22 and
111 23 (1996, plotted in orange), and cycles 23 and 24 (2008, plotted in red). The values of
112 Rz_{12} and IG_{12} for the same three periods are plotted in panels (b) and (c), respectively.
113 All three indices show that solar activity is deeper and longer than in previous years.

114 A sample portion of the data used in this study (~ 3 consecutive orbits) is shown in
115 Figure 2. The CINDI measurements are shown as solid lines, the predicted IRI-2007 values
116 are shown as dashed lines. Two examples are given to illustrate the effect of precession
117 on the density variations: the 17 Nov event (a) shows three consecutive orbits during a
118 period when perigee is near local noon; the 19 Dec event (b) shows a similar section of
119 data when perigee is near local midnight. Note that the CINDI measurements are more
120 variable than the IRI predictions.

3. Technique for Reconstructing Topside Profiles

121 The density measurements from C/NOFS are averaged together to create climatological
122 altitude profiles. Because the elliptical orbit precesses through a variety of longitudes,
123 the reconstructed profiles cannot be thought of as the ionospheric profile at any given
124 location. Rather, these are average profiles that neglect longitudinal variations, tidal
125 effects and local magnetic anomalies. (Such effects are small relative to the altitude and
126 local time effects and will be the topic of a future study.) In order to be certain that any
127 comparisons between the data and model are on equal footing, the algorithms used to

128 reconstruct average topside profiles from the CINDI data are also used on the expected
129 density values generated by IRI along each orbit of C/NOFS as shown in Figure 2.

130 The C/NOFS satellite undergoes a complete precession of perigee through all local
131 times roughly once every 65 days. In order to better smooth out the variations due to
132 the daily longitudinal precession, a period of 91 days is used for the reconstructed topside
133 data. Data that is noisy or contains localized features such as plasma density depletions or
134 enhancements are removed from the averages in order to approximate a true background
135 density. To accomplish this, a Savitsky-Golay filter [*Savitsky and Golay, 1964*] is used on
136 the C/NOFS data to determine the smoothness of the dataset. The smoothing window is
137 241 points wide (containing roughly two minutes of data), and the smoothing function is a
138 third-degree polynomial. Because the filtered values represent an average of the perturbed
139 and background densities, filtered values that differ by more than 0.5% from the measured
140 value are removed from the averages.

141 The profiles are calculated every 0.5 hours in local time with a 10 km resolution. To
142 smooth out the data, there is a significant overlap between each bin. (The bins are 2.5
143 hours wide and 50 km high.) Only points within ± 2.5 deg magnetic dip latitude are used
144 in the reconstruction, but all longitudes are used in the averages. To remove the effects
145 of magnetic substorms, only quiet times where $K_p \leq 3$ are used.

146 Figure 3a shows a sample dayside profile for the December Solstice of 2008 as recon-
147 structed from CINDI data (shown in black) and from the IRI predictions (shown in green).
148 The dashed lines represent the first and third quartiles for each bin. Part of this vari-
149 ation in the data set is due to the longitudinal variations. A sample post-sunset profile is
150 shown in Figure 3b. Note that there is a sharp in the vertical gradient for the measured

151 profile, while the IRI prediction varies smoothly. A similar effect was observed for higher
152 magnetic latitudes in *Sibanda and McKinnell* [2011].

153 Figure 4 shows the average composition associated with the profiles in Figure 3. The
154 solid lines represent the measured components of H^+ (red) and O^+ (blue), and the dashed
155 lines represent the IRI expectations. Note that for both the dayside and nightside profiles,
156 the measured concentration of O^+ is consistently lower than the expected value. This is
157 consistent with previous findings that the ionosphere is contracted more than expected
158 in the recent solar minima [*Heelis et al.*, 2009; *Lühr and Xiong*, 2010]. However, the H^+
159 component may be either larger or smaller than expected; it is consistently larger on the
160 dayside profile in the altitude range of the C/NOFS satellite.

161 The transition height between O^+ and H^+ can be inferred from the figure by noting
162 where the red curve crosses the blue curve for a given profile. The transition height for
163 the CINDI profile in Figure 4b is is ~ 50 km lower than the expected value based on IRI.
164 This is consistent with the findings by *Heelis et al.* [2009] that the transition height is
165 lower than expected during the recent solar minimum.

166 Figure 5 shows the composition profiles for the December solstice of 2010, two years
167 after the deepest part of the recent solar minimum. The estimates of both components
168 match the IRI predictions much better for the dayside profiles (5a), as well as the O^+
169 component for the post-sunset profile (5b). The H^+ component is low by a factor of 4 for
170 the upper altitudes.

171 Density and composition profiles as shown in Figures 3-4 are generated for every 0.5
172 hours of local time for 91-day seasons ranging from the December solstice of 2008 to the
173 December solstice of 2010. The variations of the topside density profiles with respect to

174 local time and season are discussed in the following two sections. The seasonal divisions
175 and the associated average solar indices are listed in Table 1. (The final season is cut
176 short by 4 days due to the current availability of definitive values for the RZ_{12} and IG_{12}
177 indices for driving the IRI model). The two equinoctial seasons remain separate in order
178 to better capture the effects of the slowly increasing solar activity.

4. Variation with Local Time

179 Figure 6 is the summary plot for the December Solstice of 2008. (This corresponds
180 to the deepest part of the cycle 23/24 minimum.) Panel (a) shows the average total
181 density as measured by CINDI as a function of altitude and solar local time, and panel (b)
182 shows the equivalent average from the IRI-2007 values generated over the C/NOFS orbits.
183 The transition height between H^+ and O^+ as calculated from the average reconstructed
184 profiles is plotted over the contour maps as a solid (CINDI) or a dashed (IRI) black line.
185 Figure 6c is the ratio of the IRI average density to that computed from CINDI. (Both
186 the measured and modeled transition heights are included in this panel for reference.)
187 Similarly reconstructed profiles for the concentrations of O^+ and H^+ are shown in Figures
188 6d-i.

189 Note that over the full range of altitudes and local times covered by the C/NOFS
190 satellite, there can be found regions where the IRI-2007 model will either overestimate
191 or underestimate density, whether it be total density (panel c), O^+ concentration (f),
192 or H^+ concentration (i). *Lühr and Xiong* [2010] found that IRI tended to overestimate
193 total density during solar min; this study was conducted with the CHAMP and GRACE
194 satellites, which are in circular orbits at 310 and 490 km altitude, respectively. Similarly,
195 for a fixed local altitude near the C/NOFS perigee, Figure 6c shows that the IRI model

196 overestimates total density for all local times except near the dawnside terminator. Av-
197 eraging over all local times at 490 km, IRI overestimates the C/NOFS density by about
198 80% for this time period, which is consistent with the GRACE results.

199 Several additional features of the contracted ionosphere are clearly seen in Figure 6. In
200 particular, the post-sunset electron density is lower than predicted by up to a factor of 4
201 (6c), and the concentration of O^+ is generally smaller than predicted for all local times
202 (6f), except near the dawnside terminator. The measured concentration of H^+ is larger
203 than estimated by IRI on the dayside profiles and for the nightside below the transition
204 height.

205 Figures 7 and 8 show similar density maps for the December solstices of 2009 and 2010,
206 respectively. It is readily apparent that the densities for the March equinox of 2010 are
207 much closer to the expected values. For instance, both the ratio plots for total density (c)
208 and O^+ concentration (e) are significantly closer to one when compared to the previous
209 year. However, there are still some discrepancies between model and data, such as near
210 sunrise and above the transition height post sunset. The estimates of H^+ for 2010 are
211 high on the nightside and low on the dayside.

5. Variation with Season and Solar Activity

212 Climatological maps similar to those shown in Figures 6-8 were generated for each
213 season shown in Table 1. In order to better illustrate the effects of seasons and solar
214 activity, certain metrics will be adopted. Figure 9 shows the vertical “total electron
215 content” (TEC) between 400 and 800 km. (This should not be confused with the total
216 electron content in the typical sense, since we only observe over a relatively small range of
217 altitudes above the F2-peak. However, it is instructive to display the relative changes in

218 this metric.) Because the height of apogee drops over the lifetime of the satellite (822 km
219 as of 31 January 2011), 800 km was chosen as the upper limit for the integrated density
220 measurements for the purposes of this metric (although the total density above 800 km is
221 minimal). The integrated vertical density is plotted in TEC units (TECU), or units of 10^{16}
222 m^{-3} . Each panel represents a given season and contains the $\text{TEC}_{400-800}$ calculated from
223 the CINDI measurements for each available year plotted as solid lines, with data from
224 2008 plotted in green, 2009 in purple, and 2010 in orange. The corresponding $\text{TEC}_{400-800}$
225 as calculated from IRI-2007 is shown in dashed lines.

226 The measured densities are significantly lower for all local times through the December
227 solstice of 2009. For the March equinox of 2010 (the orange line in Figure 9c), the
228 integrated density is $\sim 25\%$ larger than the model on the dayside. For the two following
229 seasons in 2010, the modeled values better approximate the CINDI measurements than in
230 the previous seasons. Additionally, the CINDI measurements in the December solstice of
231 2009 are still very close to those from 2008, while there is a dramatic increase in density for
232 the March equinox of 2010. This corresponds to a rise in F10.7 above 80 sfu. Additionally,
233 the average effective sunspot number (IG_{12}) based on the ionospheric activity more closely
234 matches the measured sunspot number (Rz_{12}) for this period.

235 Another interesting feature is that the measured ion density in March equinox of 2010
236 is larger than the corresponding density in the September equinox of the same year. The
237 TEC plots from these two periods have been replotted in a single panel in Figure 10 to
238 better illustrate this asymmetry. All three of the solar/ionospheric activity proxies are
239 larger in for the September equinox than the March period (see Table 1). Accordingly,
240 the IRI-2007 modeled values predict that the densities in September would be larger (the

241 dashed orange lines) than those from March (dashed purple lines). This is clearly not the
242 case in the measured densities (represented by the solid lines). This equinoctial asymmetry
243 is similar to that noted in the COSMIC TEC data by *Liu et al.* [2010]. A similar effect
244 was recently reported in the vertical drift data from the ROCSAT-1 satellite [*Ren et al.*,
245 2011]. However, we should remember that the ROCSAT data is from a period when
246 the solar activity was much higher, and an investigation into this equinoctial asymmetry
247 utilizing the C/NOFS vertical drift data will be required to fully understand this ion
248 density asymmetry.

249 The transition height between H^+ and O^+ is calculated from the reconstructed profiles
250 for both data and model. These are shown with respect to seasonal and temporal vari-
251 ations in Figure 11 (similar to the integrated densities presented previously). Note that
252 there is no significant difference between the nightside transition height as predicted by
253 IRI over the course of the mission (the dayside transition heights are typically outside
254 of the range of the C/NOFS satellite). The dayside transition heights for 2010 are still
255 lower than predicted by the models, but it should be noted that these are consistent with
256 observations from Atmospheric Explorer from a previous solar minimum [*González et al.*,
257 1992]. The nightside transition heights for 2010 are consistent with that predicted by IRI.

6. Discussion

258 The reduced densities observed during the extreme portion of the recent solar minimum
259 could be explained by any combination of the following effects:

- 260 1. The height of the F2 layer (h_mF2) is lower than predicted.
- 261 2. The density of the F2 peak (N_mF2) is lower than predicted.

262 3. The shape of the topside ionosphere is different.

263 Because the peak of the F layer is below the C/NOFS perigee (400 km) for most of
 264 the mission, we cannot comment on the cause from this data alone. (C/NOFS travelled
 265 below the F peak for the first time in April 2011.) Figure 12 is provided to illustrate this
 266 problem. An initial ion density profile is generated from IRI-2007 (shown in black) for
 267 the December solstice of 2008 for 1400 local time. Two modified profiles are created that
 268 would lead to the observed $\sim 67\%$ overestimate in $\text{TEC}_{400-800}$ shown in Figure 9. The
 269 first is created by simply scaling the density by a factor of 0.6 (shown in blue), the second
 270 is created by moving the F peak down by 65 km (shown in red).

271 While recent studies using ionosonde data have shown that NmF2 reached record low
 272 measurements during the recent solar minimum [*Liu et al.*, 2011], IRI-2007 is found to
 273 predict this density very well, with the standard deviations being comparable to previous
 274 solar cycles [*Bilitza et al.*, 2011]. This is due to the fact that the IRI model predicts the
 275 peak density based on the IG12 index, which is in itself a global average of ionosonde
 276 measurements.

277 The topside ionospheric density is controlled not just by solar radiation, but by a balance
 278 of chemical and dynamic processes. In the topside ionosphere, the creation of H^+ ions is
 279 primarily due to charge exchange with O^+ [*Rishbeth and Garriott*, 1969].



280 To first order approximation, the relation between the the ion components will then
 281 depend on the densities of the neutral components.

$$[H^+] = \frac{9}{8} \frac{[H]}{[O]} [O^+] \quad (2)$$

282 The factor of 9/8 is due to statistical differences in the forward and reverse reaction
283 rates. The increased concentration of H^+ in the topside ionosphere is consistent with the
284 increased ratio of neutral $[H]/[O]$ observed in the upper thermosphere [*Haaser et al.*, 2010].
285 A recent study by *Hysell et al.* [2009] compared topside profiles from the Jicamarca Radar
286 Observatory with the SAMI2 model and concluded that the shape of the H^+ fraction is
287 also affected by the $\mathbf{E} \times \mathbf{B}$ drift time history as well.

288 This decreased post-sunset density may be partially related to the altered vertical drift
289 climatology during the recent solar min. Unlike the Fejer-Schierless model, the vertical
290 drift is found to be downward in the afternoon, and the large upward drift around sunset
291 known as the pre-reversal enhancement is largely absent in the 2008 and 2009 data [*Pfaff*
292 *et al.*, 2010]. The density structure may also be due to different climatologies in the
293 meridional winds.

7. Summary and Conclusions

294 A statistical study of the ion density and composition in the topside ionosphere near
295 the magnetic dip equator during the recent solar minimum was conducted. The major
296 findings are the following:

- 297 1. While the overall ionosphere was found to be contracted relative to empirical ex-
298 pectations, the ratio of the expected density to the measured density was found to be a
299 strong function of altitude and local time, including some areas (such as ~ 800 km just

300 before dawn) where the average measured ion density was higher than predicted by as
301 much as a factor of four.

302 2. During this contracted phase, $[H^+]$ is found to be greater than predicted by IRI-2007
303 for all observed altitudes (400 to 850 km) on the dayside and below the transition height
304 for the nightside.

305 3. The shape of the topside nighttime ionosphere between 400 and 850 km was found
306 to be different from the predicted shape. The profile generated by IRI varies smoothly,
307 while the data shows a sharp change in the vertical gradient associated with the lower
308 transition height.

309 4. The post-sunset ion density decreased more rapidly than expected based on previous
310 solar minima. This may be related to a different drift climatology observed with the
311 C/NOFS satellite during extreme solar min as previously reported by *Pfaff et al.* [2010].

312 5. This highly contracted ionosphere persisted until the March equinox of 2010, over a
313 year into the new solar cycle. The transition heights observed in 2010 are consistent
314 with observations from previous solar minima.

315 6. The geophysical indices used to drive the IRI model, Rz_{12} and IG_{12} , are both signif-
316 icantly lower than in previous solar minima. The previously reported tendency of IRI to
317 overestimate density during the extreme solar min is not a deficiency of the chosen input
318 indices, but rather illustrates the fact that we have not observed the ionosphere during
319 such a low period of solar activity. The reconstructed topside profiles from C/NOFS can
320 be used as an additional constraint on future versions of IRI.

321 The C/NOFS satellite provides a unique look at the shape of the topside ionosphere.
322 The topside data from C/NOFS during this unprecedented low in solar activity could

323 be used as a constraint on future empirical models. Future studies will include regional
324 case studies for comparison with ground-based measurements, as well as variations with
325 longitude and magnetic latitude. Additionally, the reconstructed profiles can be used to
326 discuss transport phenomena in the topside ionosphere in conjunction with drift clima-
327 tologies using physics-based models to quantify the relative effects of altered transport
328 and chemistry during extreme solar minimum.

329 **Acknowledgments.** JK and FS are supported by an appointment to the NASA Post-
330 doctoral Program at Goddard Space Flight Center, administered by Oak Ridge Associ-
331 ated Universities through a contract with NASA. The work performed by SI was sup-
332 ported by the NASA Undergraduate Student Research Program. The work at the Uni-
333 versity of Texas at Dallas is supported by NASA grant NAS5-01068. The Communica-
334 tion/Navigation Outage Forecast System (C/NOFS) mission, conceived and developed by
335 the Air Force Research Laboratory, is sponsored and executed by the USAF Space Test
336 Program. F10.7, R_{Z12}, and IG₁₂ are provided by the UK World Data Center.

References

- 337 Araujo-Pradere, E. A., R. Redmon, M. Fedrizzi, R. Viereck, T. J. Fuller-Rowell (2011),
338 Some Characteristics of the Ionospheric Behavior During the Solar Cycle 23 24 Mini-
339 mum, *Solar Phys.*, DOI 10.1007/s11207-011-9728-3.
- 340 Benson, R. F., and D. Bilitza (2009), New satellite mission with old data: Rescuing a
341 unique data set, *Radio Sci.*, 44, RS0A04, doi:10.1029/2008RS004036.
- 342 Bilitza, D. (2000), The importance of EUV indices for the international reference iono-
343 sphere, *Phys. Chem. Earth (C)*, 25, pp. 515-52.

- 344 Bilitza, D., B. W. Reinisch, S. M. Radicella, S. Pulinets, T. Gulyaeva, and L Triskova
345 (2006), Improvements of the International Reference Ionosphere model for the topside
346 electron density profile, *Radio Sci.*, *41*, RS5S15, doi:10.1029/2005RS003370.
- 347 Bilitza, D., and B. W. Reinisch (2008), International Reference Ionosphere 2007: Improve-
348 ments and new parameters, *Adv. Space Res.*, *43*, 599, doi:10.1016/j.asr.2007.07.048.
- 349 Bilitza, D. (2009), Evaluation of the IRI-2007 model options for the topside electron
350 density, *Adv. Space Res.*, *44*, 701, doi:10.1016/j.asr.2009.04.036.
- 351 Bilitza, D., S. A. Browna, M. Y. Wang, and P. A. Roddy (2011), Measurements and IRI
352 Model Predictions during the Recent Solar Minimum, *presented at URSI GASS 2011*,
353 Session G02.4.
- 354 Chen, Y., L. Liu, and W. Wan (2011), Does the $F_{10.7}$ index correctly describe the solar
355 EUV flux during the deep solar minimum of 2007-2009?, *J. Geophys. Res.*, *116*, A04304,
356 doi:10.1029/2010JA016301.
- 357 Clette, F., D. Berghmans, P. Vanlommel, R. A. M. Van der Linden, A. Koeckelenbergh,
358 and L. Wauters (2007), From the Wolf number to the International Sunspot Index: 25
359 years of SIDC, *Adv. Space Res.*, *40*, p 919928, doi:10.1016/j.asr.2006.12.045.
- 360 Coley, W. R., R. A. Heelis, M. R. Hairston, G. D. Earle, M. D. Perdue, R. A. Power,
361 L. L. Harmon, B. J. Holt, and C. R. Lippincott (2010), Ion temperature and density
362 relationships measured by CINDI from the C/NOFS spacecraft during solar minimum,
363 *J. Geophys. Res.*, *115*, A02313, doi:10.1029/2009JA014665.
- 364 de La Beaujardière, O., and the C/NOFS Definition Team (2004), C/NOFS:
365 a mission to forecast scintillations, *J. Atmos. and Sol-Terr. Phys.*, *66*, 1573,
366 doi:10.1016/j.jastp.2004.07.030.

- 367 Emmert, J. T., J. L. Lean, and J. M. Picone (2010), Record-low thermo-
368 spheric density during the 2008 solar minimum, *Geophys. Res. Lett.*, *37*, L12102,
369 doi:10.1029/2010GL043671.
- 370 González, S. A., B. G. Fejer, R. A. Heelis, and W. B. Hanson (1992), Ion Composition
371 of the Topside Equatorial Ionosphere During Solar Minimum, *J. Geophys. Res.*, *97*, pp
372 4299-4303.
- 373 Greenspan, M. E., W. J. Burke, F. J. Rich, W. J. Hughes, and R. A. Heelis, DMSP F8 ob-
374 servations of the mid-latitude and low-latitude topside ionosphere near solar minimum,
375 *J. Geophys. Res.*, *99*, pp 3817-3826.
- 376 Haaser, R. A., G. D. Earle, R. A. Heelis, W. R. Coley, and J. H. Klenzing (2010), Low-
377 latitude measurements of neutral thermospheric helium dominance near 400 km during
378 extreme solar minimum, *J. Geophys. Res.*, *115*, A11318, doi:10.1029/2010JA015325.
- 379 Heelis, R. A., and W. B. Hanson (1998), "Measurements of thermal ion drift velocity
380 and temperature using planar sensors," in *Measurement Techniques in Space Plasmas*
381 (*Geophys. Monogr. Ser. vol. 102*), edited by R. F. Pfaff, J. E. Borovsky, and D. T.
382 Young, (AGU, Washington, D. C., 1998) p. 61.
- 383 Heelis, R. A., W. R. Coley, A. G. Burrell, M. R. Hairston, G. D. Earle, M. D. Perdue,
384 R. A. Power, L. L. Harmon, B. J. Holt, and C. R. Lippincott (2009), Behavior of the
385 O⁺/H⁺ transition height during the extreme solar minimum of 2008, *Geophys. Res.*
386 *Lett.*, *36*, L00C03, doi:10.1029/2009GL038652.
- 387 Hysell, D. L., J. L. Chau, and J. D. Huba (2009), Topside measurements at
388 Jicamarca during solar minimum, *Ann. Geophys.*, *27*, pp 427439, www.ann-
389 geophys.net/27/427/2009/.

- 390 Liu, R. Y., P. A. Smith, and J. W. King (1983), A new solar index which leads to improved
391 foF2 predictions using the CCIR Atlas, *Telecomm. J.*, *50*, p 408.
- 392 Liu, L., M. He, X. Yue, B. Ning, and W. Wan (2010), Ionosphere around equinoxes during
393 low solar activity, *J. Geophys. Res.*, *115*, A09307, doi:10.1029/2010JA015318.
- 394 Liu, L., Y. Chen, H. Le, V. I. Kurkin, N. M. Polekh, and C.-C. Lee (2011), The iono-
395 sphere under extremely prolonged low solar activity, *J. Geophys. Res.*, *116*, A04320,
396 doi:10.1029/2010JA016296.
- 397 Lühr, H., and C. Xiong (2010), IRI-2007 model overestimates electron density during the
398 23/24 solar minimum, *Geophys. Res. Lett.*, *37*, L23010, doi:10.1029/2010GL045430.
- 399 Minnis, C., and G. Bazzard (1960), A monthly ionospheric index of solar activity
400 based on F2-layer ionisation at eleven stations, *J. Atmos. Terr. Phys.*, *18*, p 297-305,
401 doi:10.1016/002191696091136.
- 402 Pfaff, R., D. Rowland, H. Freudenreich, K. Bromund, G. Le, M. Acuña, J. Klenz-
403 ing, C. Liebrecht, S. Martin, W. J. Burke, N. C. Maynard, D. E. Hunton, P. A.
404 Roddy, J. O. Ballenthin, and G. R. Wilson (2010), Observations of DC Electric Fields
405 in the Low Latitude Ionosphere and Their Variations with Local Time, Longitude,
406 and Plasma Density during Extreme Solar Minimum, *J. Geophys. Res.*, *115*, A12324,
407 doi:10.1029/2010JA016023.
- 408 Ren, Z., W. Wan, L. Liu, Y. Chen, and H. Le (2011), Equinoctial asymmetry of ionospheric
409 vertical plasma drifts and its effect on F-region plasma density, *J. Geophys. Res.*, *116*,
410 A02308, doi:10.1029/2010JA016081.
- 411 Rishbeth, H., and O. K. Garriott (1969), "Introduction to ionospheric physics," Academic
412 Press, New York, NY.

- 413 Russell, C. T., J. G. Luhmann, and L. K. Jian (2010), How unprecedented a solar mini-
414 mum?, *Rev. Geophys.*, *48*, RG2004, doi:10.1029/2009RG000316.
- 415 Savitzky, A., and M. J. E. Golay (1964), Smoothing and differentiation of data by sim-
416 plified least squares procedures, *Anal. Chem.*, *36*, p1627.
- 417 Scherliess, L. and B. G. Fejer (1999), Radar and satellite global equatorial F region vertical
418 drift model, *J. Geophys. Res.*, *104*, p 6829-6842.
- 419 Schrivjer, C. J., W. C. Livingston, T. N. Woods, and R. A. Mewaldt (2011), The minimal
420 solar activity in 2008-2009 and its implications for long-term climate modeling, *Geophys.*
421 *Res. Lett.*, *38*, L06701, doi:10.1029/2011GL046658.
- 422 Sibanda, P., and L. A. McKinnell (2011), Topside ionospheric vertical electron density
423 profile reconstruction using GPS and ionosonde data: possibilities for South Africa,
424 *Ann. Geophys.*, *29*, 229236, doi:10.5194/angeo-29-229-2011
- 425 Solomon, S. C., T. N. Woods, L. V. Didkovsky, J. T. Emmert, and L. Qian (2010),
426 Anomalously low solar extreme-ultraviolet irradiance and thermospheric density during
427 solar minimum, *Geophys. Res. Lett.*, *37*, L16103, doi:10.1029/2010GL044468.
- 428 Solomon, S. C., L. Qian, L. V. Didkovsky, R. A. Viereck, and T. N. Woods (2011), Causes
429 of low thermospheric density during the 2007-2009 solar minimum, *J. Geophys. Res.*,
430 *116*, A00H07, doi:10.1029/2011JA016508.
- 431 West, K. H., R. A. Heelis, and F. J. Rich (1997), Solar activity variations in
432 the composition of the low latitude ionosphere, *J. Geophys. Res.*, *102*, 295305,
433 doi:10.1029/96JA03031.

Table 1. Seasonal divisions for the topside profile reconstructions, including the average solar activity represented by F10.7, RZ₁₂, and IG₁₂ for each period.

Period	Range of Days	F10.7	RZ ₁₂	IG ₁₂
Sep Equinox 2008	8 Aug 2008 – 6 Nov 2008	67.8	2.3	-10.1
Dec Solstice 2008	6 Nov 2008 – 4 Feb 2009	67.3	2.0	-9.2
Mar Equinox 2009	3 Feb 2009 – 4 May 2009	69.2	2.0	-8.4
Jun Solstice 2009	7 May 2009 – 5 Aug 2009	70.9	3.2	-6.3
Sep Equinox 2009	8 Aug 2009 – 6 Nov 2009	70.9	6.2	-0.8
Dec Solstice 2009	6 Nov 2009 – 4 Feb 2010	75.5	8.5	3.9
Mar Equinox 2010	3 Feb 2010 – 4 May 2010	80.3	12.5	10.3
Jun Solstice 2010	7 May 2010 – 5 Aug 2010	77.9	16.8	15.7
Sep Equinox 2010	8 Aug 2010 – 6 Nov 2010	81.5	21.0	19.0
Dec Solstice 2010	6 Nov 2010 – 31 Jan 2011	81.6	29.1	26.2

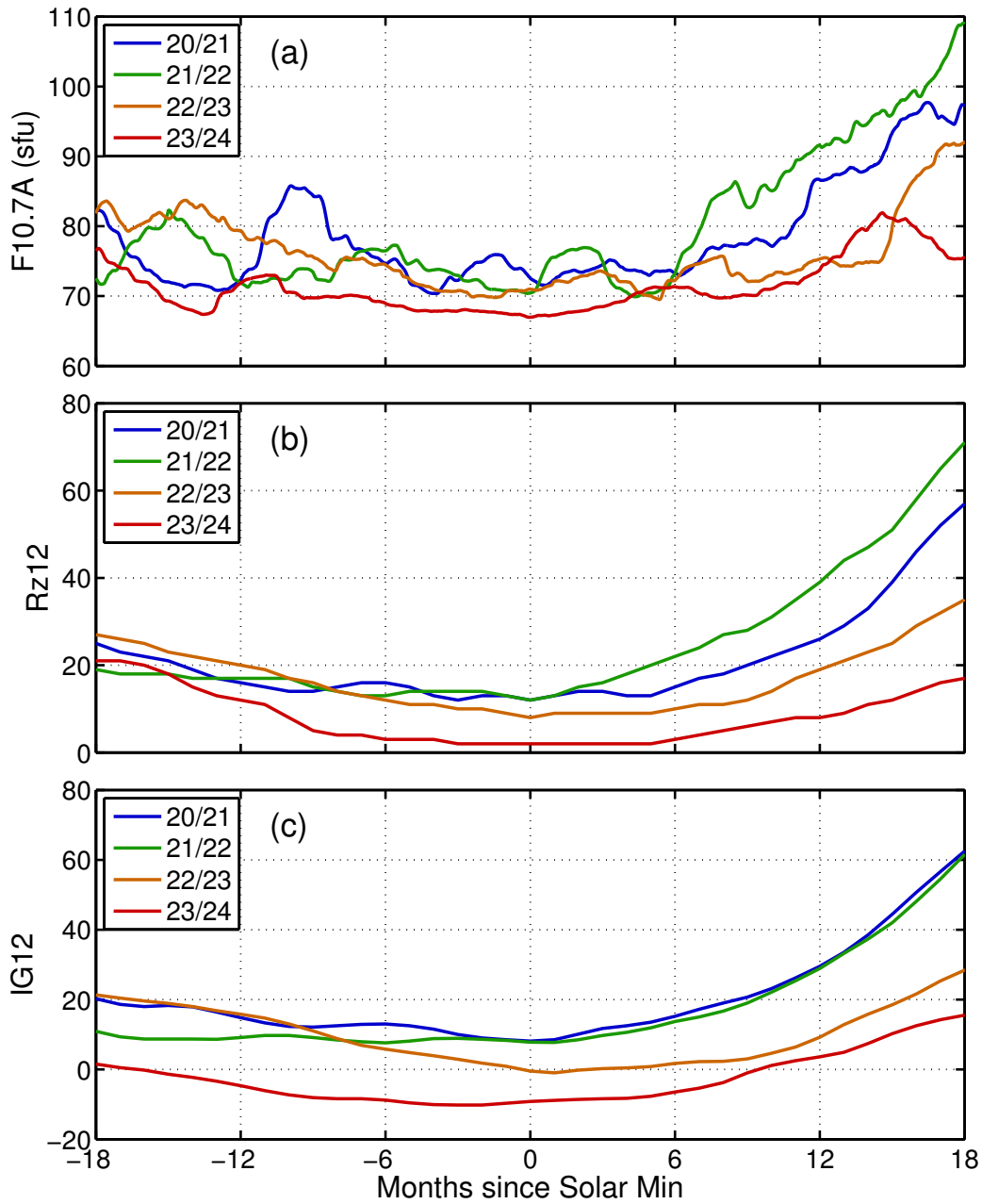


Figure 1. Solar activity near the solar minima for the last three cycles, including (a) F10.7A, (b) Rz_{12} , and (c) IG_{12} . The F10.7A values are 81-day averages, and the Rz_{12} and IG_{12} indices are 12-month averages. Rz_{12} and IG_{12} are used to drive the IRI-2007 model in this study.

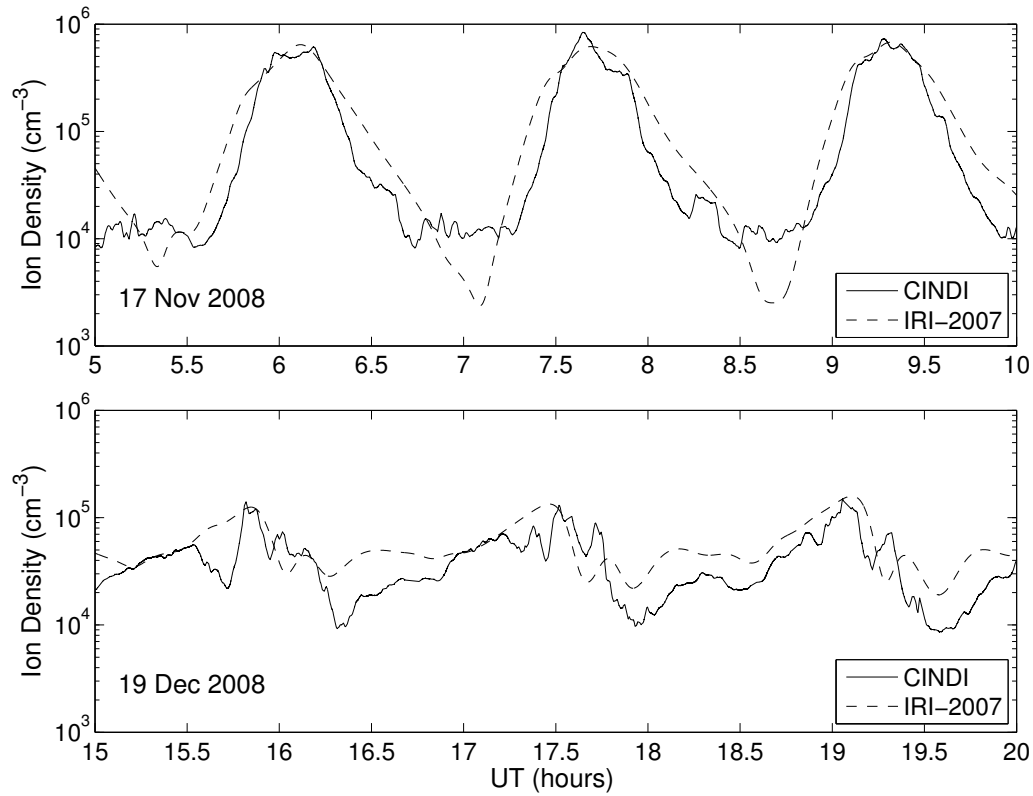


Figure 2. The variability of C/NOFS density data, along with the expected values based on IRI-2007. The top panel shows five hours (roughly three orbits) from 17 Nov 2008 (when perigee is at local noon), and the bottom panel shows the same for 19 Dec 2008 (when perigee is at local midnight)

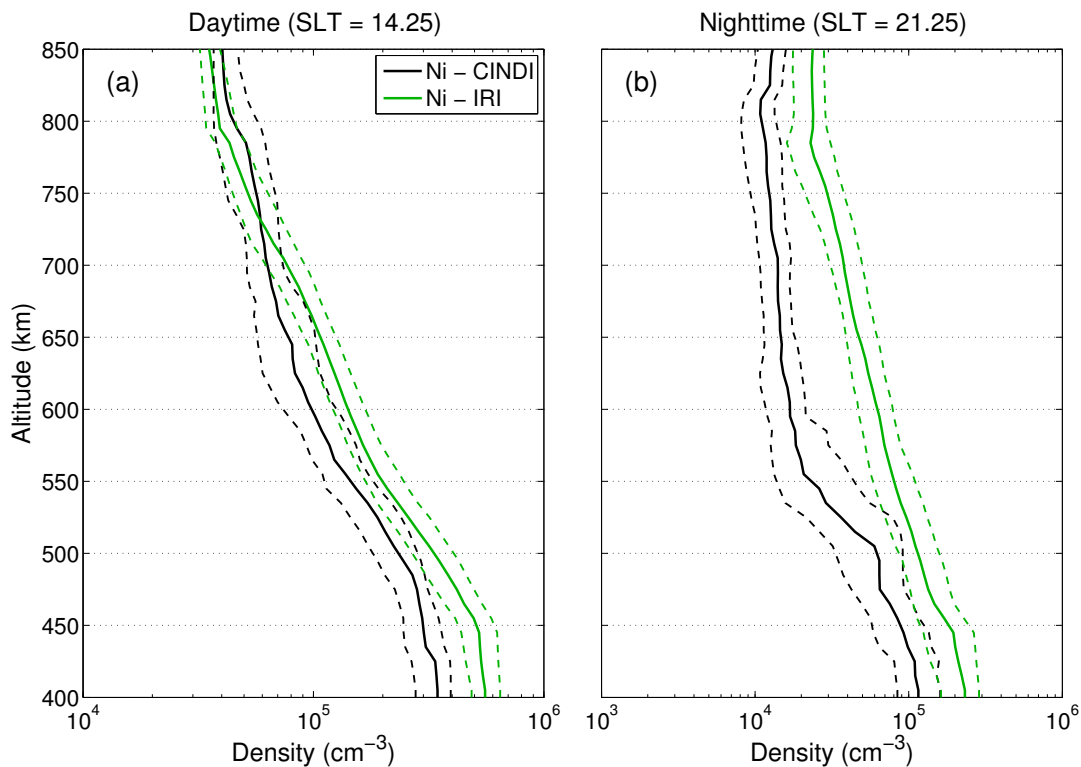


Figure 3. A sample reconstructed altitude profile based on the average C/NOFS CINDI data (black) for the topside equatorial ionosphere for the December solstice of 2008, along with the associated IRI-2007 profile (green). The solid lines represent the median density profile; the dashed lines represent the first and third quartiles. The left panel is a dayside profile, centered around 14.25 local time; and the right panel is a nightside profile, centered around 21.25 local time.

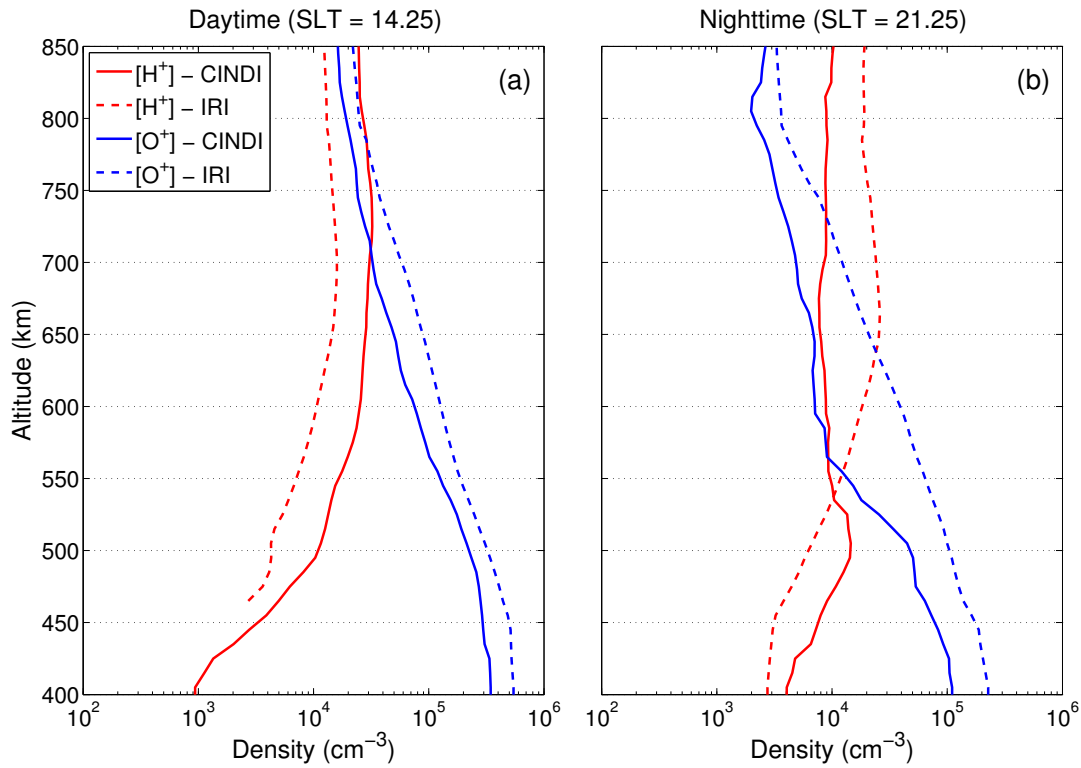


Figure 4. The composition profiles associated with the density profiles from Figure 3. The two major component ions are H^+ (red) and O^+ (blue). Note that while the total ion density matched IRI quite well for the dayside profiles, the composition is quite different. For both dayside and nightside, the transition height between H^+ and O^+ is lower than predicted.

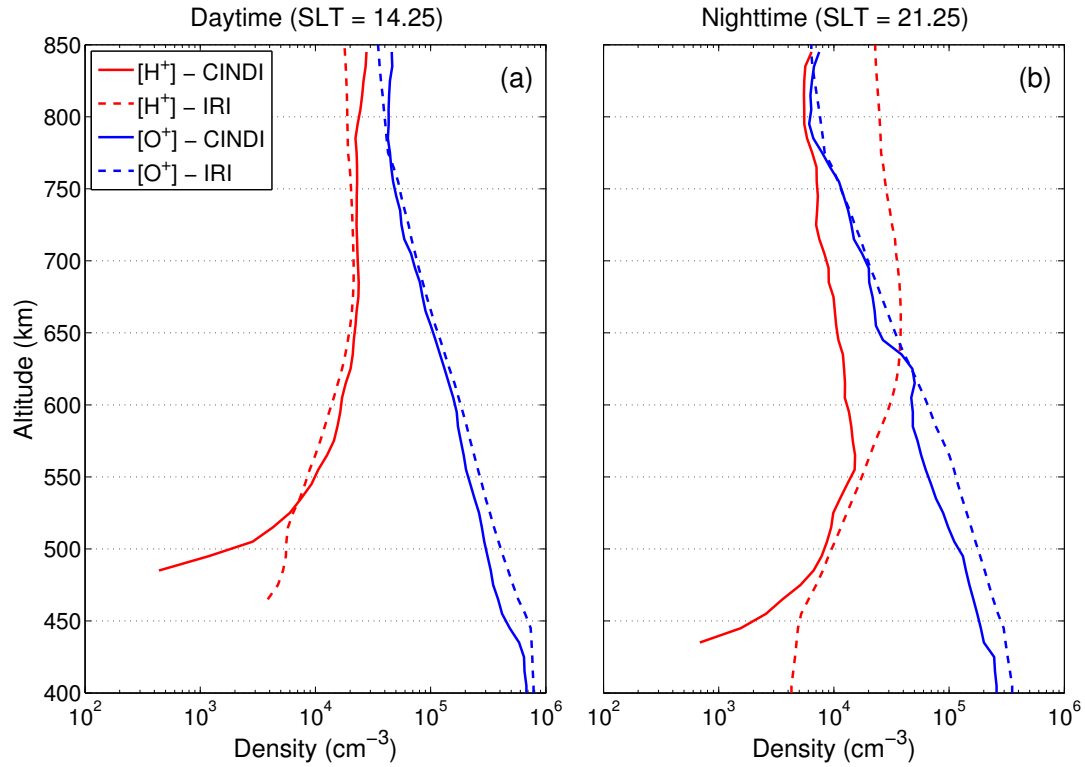


Figure 5. The same as Figure 4, but for the December solstice of 2010 (2 years later). Note that the nightside transition height between O^+ and H^+ is now very similar for both the measurements and the model.

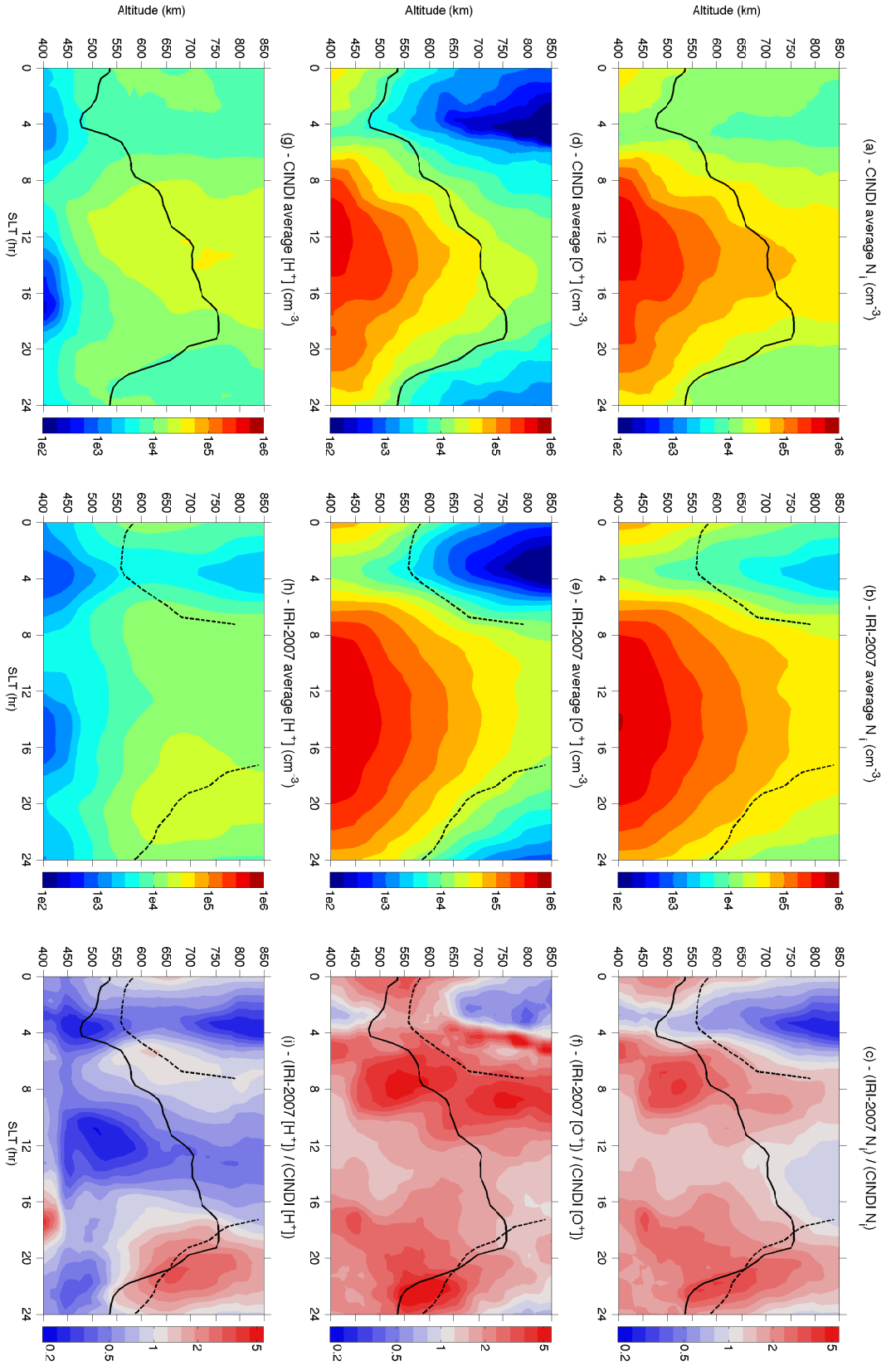


Figure 6. The average total and component densities as a function of altitude and local time for the December solstice

2008. Panel (a) shows the average total ion density, while panel (b) shows the average expected densities based on IRI-2007.

Panel (c) is the ratio of the expected density to the measured values. The other rows show the same for the O⁺ component (d-f) and the H⁺ component (g-i).

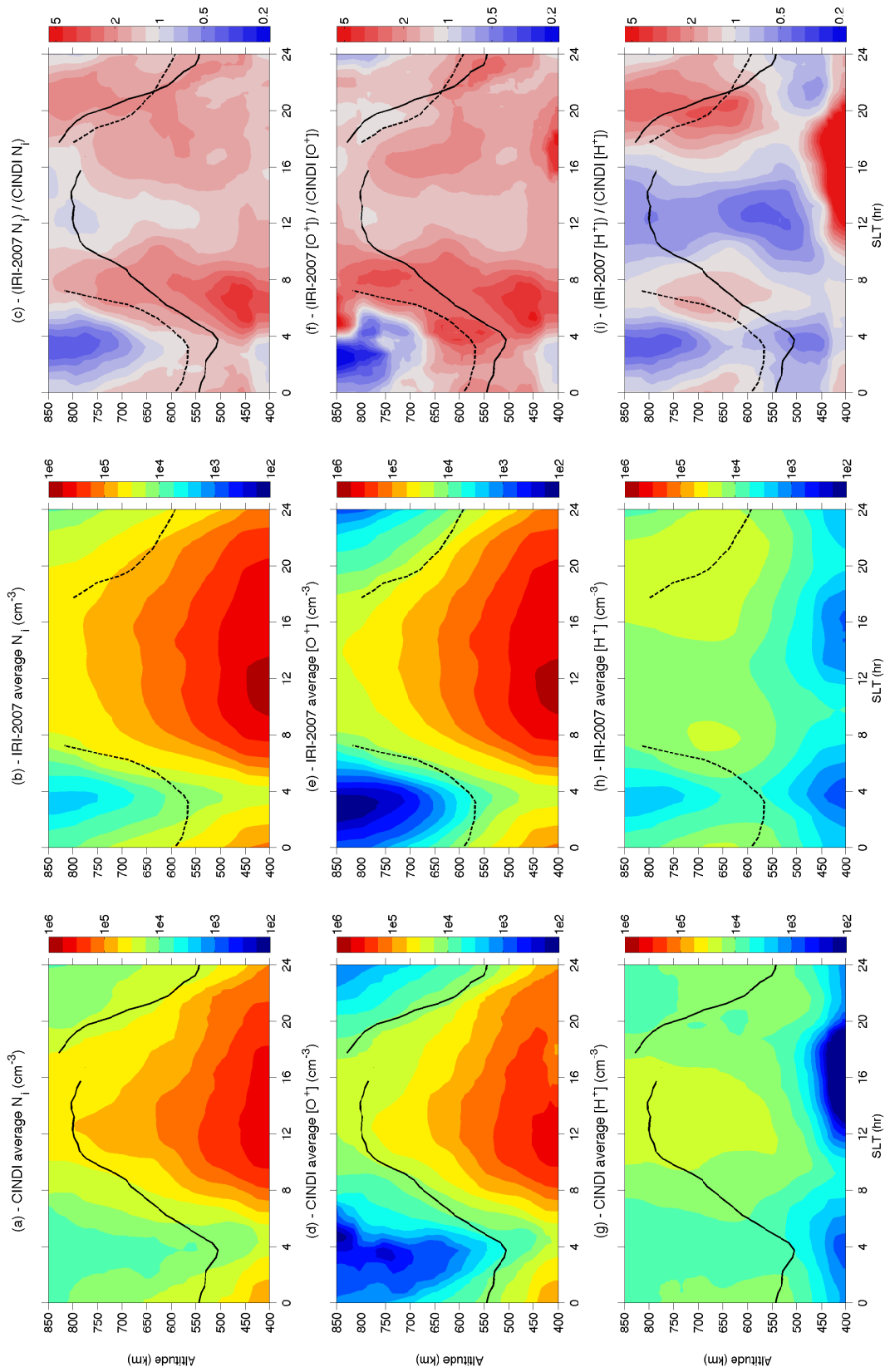


Figure 7. The average total and component densities as a function of altitude and local time for the December solstice 2009. The format is the same as in Figure 6.

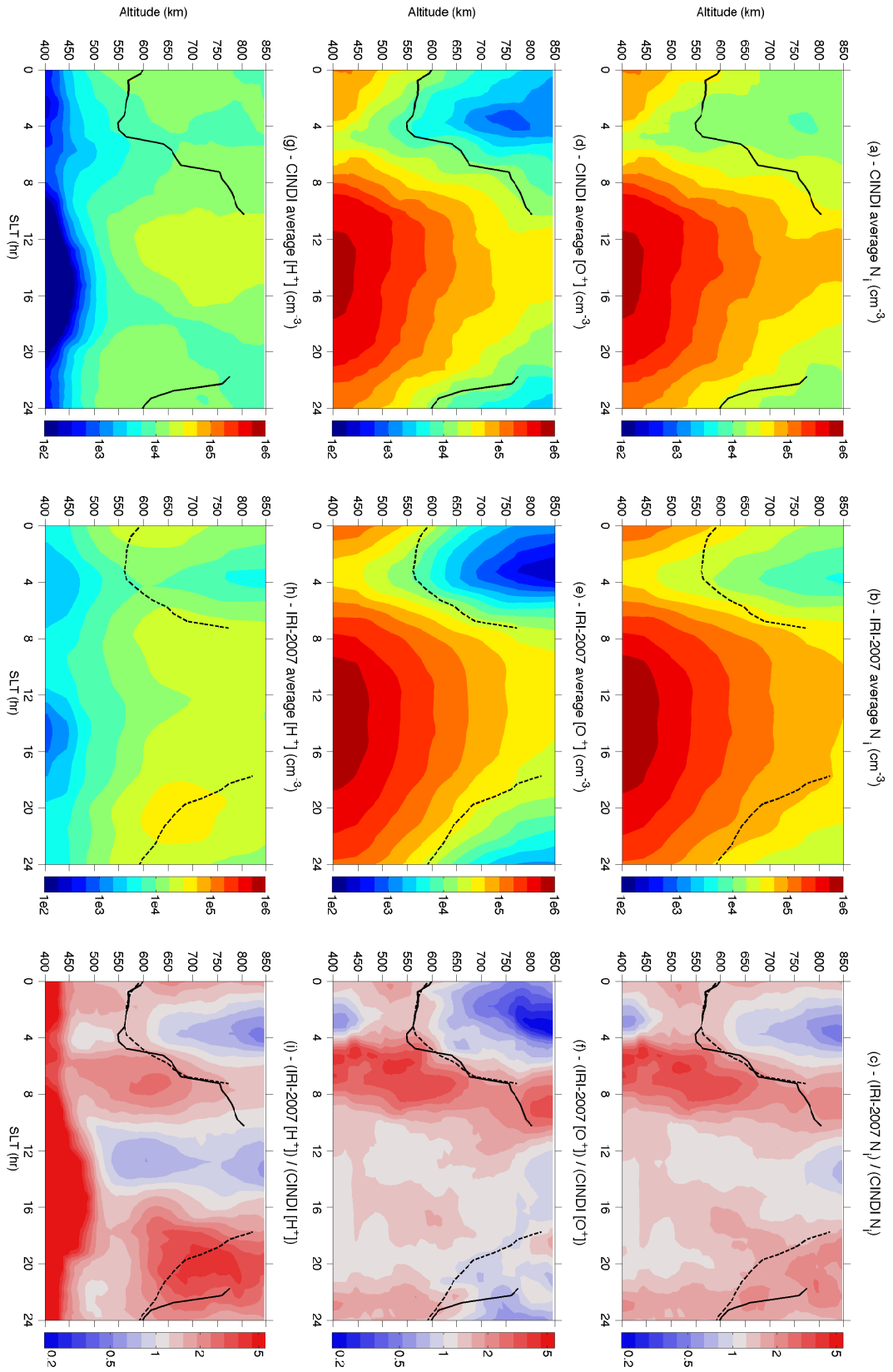


Figure 8. The average total and component densities as a function of altitude and local time for the December solstice

2010. The format is the same as in Figure 6.

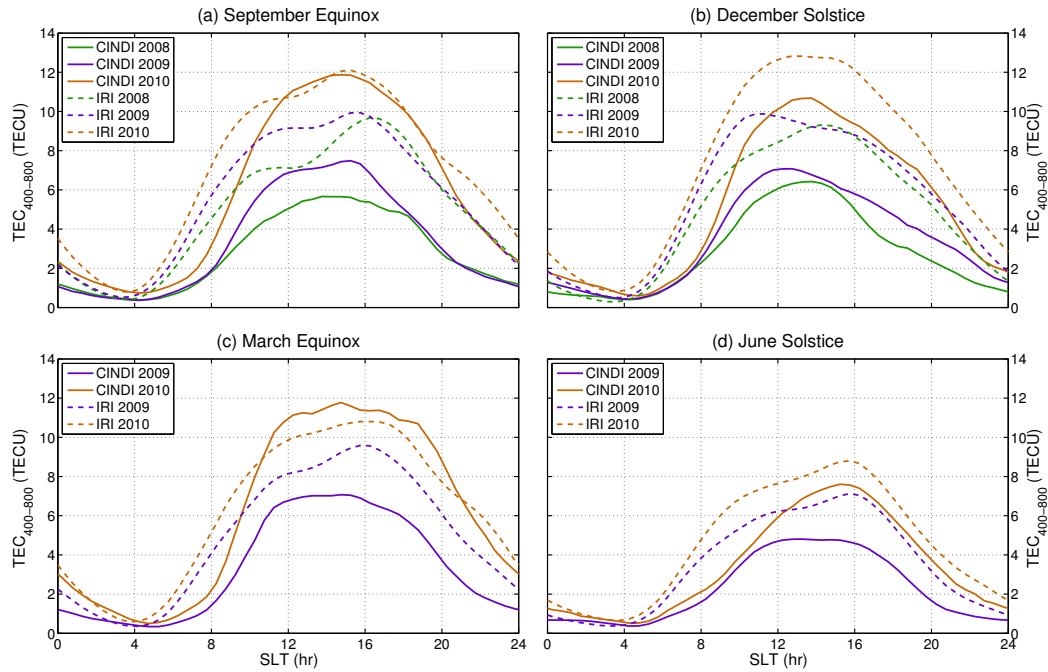


Figure 9. The “total” electron content between 400 and 800 km as a function of solar local time. These plots capture the seasonal and temporal variation of density for (a) September equinox, (b) December solstice, (c) March equinox, and (d) June solstice. Note that the measured densities are significantly lower than predicted by IRI until the March equinox of 2010.

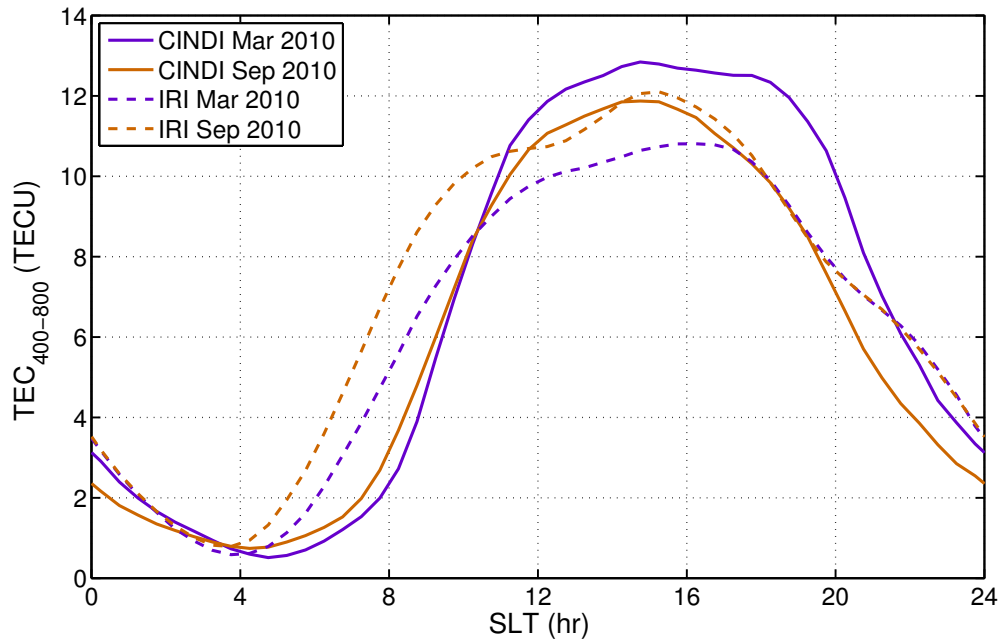


Figure 10. Selected data from Figure 9 replotted to illustrate the equinoctial asymmetry during 2010. The March equinox TEC is larger than the corresponding data in the September Equinox after ~ 10.5 SLT.

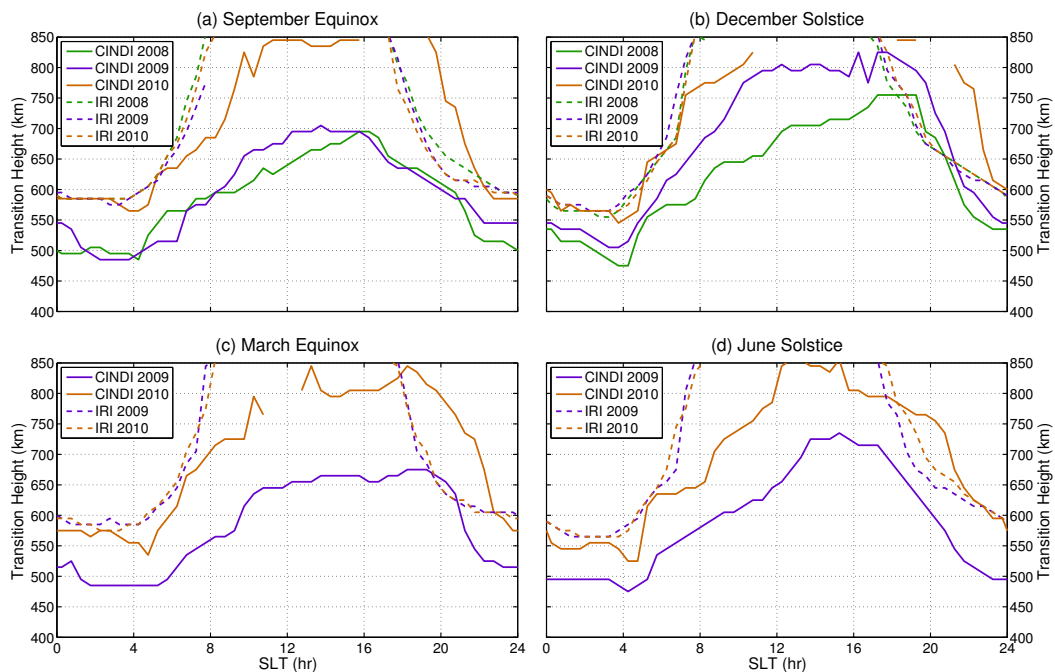


Figure 11. The transition height between H^+ and O^+ as a function of solar local time. These plots capture the seasonal and temporal variation for (a) September equinox, (b) December solstice, (c) March equinox, and (d) June solstice. Note that the daytime transition height as predicted by IRI is above the range of the C/NOFS satellite.

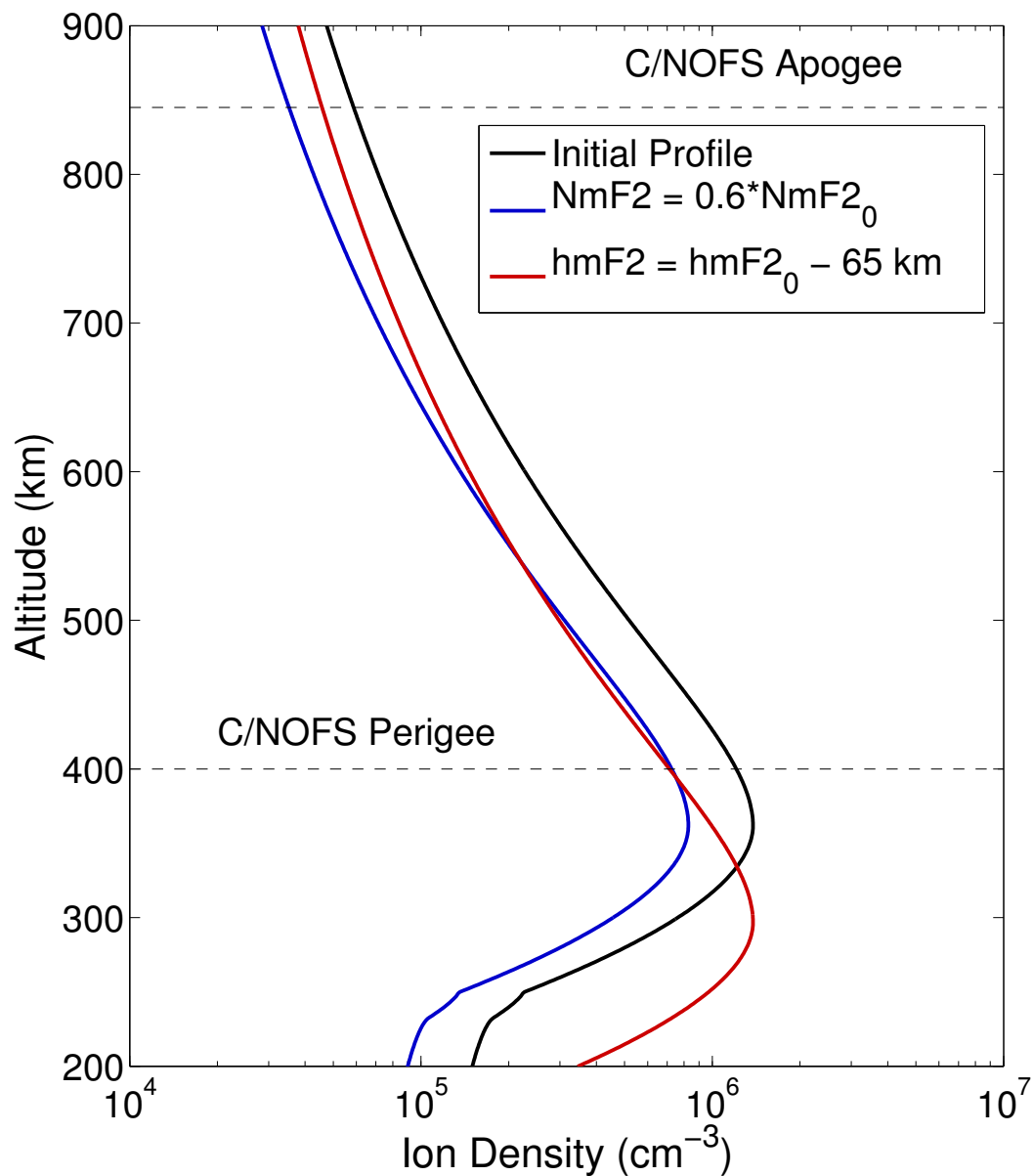


Figure 12. The effects of changing the position of the F -peak on the observed topside profile. An initial profile (black) is generated using IRI-2007. Two altered profiles are included: one where $NmF2$ is scaled down by 60% (blue), and one where $hmF2$ is moved down by 65 km. The apogee and perigee of the C/NOFS satellite are shown as dashed lines.